Morphological and micro-structural interface characterization in multilayer inverted polymer-fullerene bulk heterojunction solar cells

A. Jouane[a], R. Moubah[a], G. Schmerber[b], R. Lardé[c], Y. Odarchenko[d,g], D. A. Ivanov[d,f], H. Lassri[a], Y. -A, Chapuis[e], Y. Jouane[b,e,*]

[a]LPMMAT, Faculté des Sciences Ain Chock, University Hassan II of Casablanca, Morocco.
[b]Université de Strasbourg, CNRS, IPCMS, UMR 7504, F-67000 Strasbourg, France.
[c]Groupe de Physique des Matériaux, UMR 6634 CNRS, Université et INSA de Rouen, Avenue de l'Université, BP 12, 76801 Saint Etienne du Rouvray Cedex, France
[d]IS2M, Institut de Sciences des Matériaux de Mulhouse, UMR 7361 CNRS-UHA, 15 Rue Jean Starcky, BP 2488, 68057 Mulhouse Cedex, France
[e]Université de Strasbourg, CNRS, ICube, UMR 7357, F-67000 Strasbourg, France
[f]Moscow Institute of Physics and Technology (State University), Institutskiy per. 9, Dolgoprudny, 141700, Russia
[g]Department of Chemistry, University College London, 20 Gordon Street, London, WC1H 0AJ, UK

Abstract

Inverted polymer solar cells based on P3HT/PCBM bulk heterojunction were prepared on flexible polyethylene naphthalate (PEN) substrate. The effect of annealing of the PEN/ITO/ZnO multilayer and ZnO/P3HT:PCBM on the structural, morphological, photophysical and photovoltaic properties was investigated and scrutinized directly on the OPV devices using atom probe tomography (APT), scanning electron microscopy (SEM) and microfocus X-rays techniques. We carried out a 3D reconstruction of the interfaces of the multilayer containing PEN/ITO, ZnO/ITO and P3HT:PCBM/ZnO to address the interface micro-structure and its influence on the morphology of the photoactive film. The analyses show that the morphology of the interfaces is affected by the structure of each layer of the BHJ devices causing orientation of P3HT crystals with PCBM aggregates and ZnO, which in turn leads to a significant change of the charge transport across each layer and therefore photovoltaic performances.

Keywords: Atom Probe Tomography, Organic/Inorganic Heterostructures, Interface characterization, Flexible polymer-fullerene bulk heterojunction solar cells, Synchrotron micro-focus X-ray diffraction, Photoluminescence spectroscopy, Charge transfer.

1. Introduction

Flexible electronics holds a great promise for the development of future electronic devices.[1, 2] However, there are technological barriers which have still to be overcome for spreading their integration. The progress of **power conversion efficiency (PCE)** record is stimulated by the synthesis of new donor and acceptor materials, implementation of new interfacial materials and also the analysis and control of each interface in the bulk hetero-junction (BHJ) structure[3]. The interfaces between organic polymers, metals and interfacial layers are often problematic since an interface with a barrier height of a few tens of mV can result in significant charge build-up and therefore significant loss of recombination and photovoltaic performance. In addition, the inevitable potential loss due to the shift of the energy level at the interface between the donor and the acceptor renders the electrode contacts critical factor to derive the net potential out of the BHJs. Therefore, the interface between the BHJ and both the anode and the cathode is of critical importance for charge transport and the extraction process, which determines device performance and long-term interfacial stability. Quantitative analysis of these interfaces is one of the keys to controlling the processing parameters, structure and performance of the final device. However, the interfacial analysis is challenging due to the complex chemistry of these interfaces. We note that nano-SIMS [4] is an interesting technique, which provides chemical details, whereas good-resolution imaging can be obtained in the energy-filtered transmission electron microscopy (EFTEM)[5].**However, laser-pulsed atom probe tomography (APT) combines sub-nanometer resolution with chemical sensitivity across the interface organic/inorganic. furthermore, APT is the only analysis technique offering extensive capabilities for both 3D imaging and chemical composition measurements at the atomic scale. Contrary to EDS which is limited for the light elements. APT can detect and quantify all elements (even hydrogen) present in the analysed material in the device structure with high sensi-**

*Corresponding author
  Email address: yjouane@hotmail.fr (Y. Jouane)

tivity (about 50 ppm). However TEM or STEM analyses can provide complementary informations about crystal structure.

Considerable efforts have been devoted to the analysis and elucidation of the problems caused by interfaces since the evolution of polymer solar cells, but it is only recently that it begins to evoke the morphology and the modification of the structure of each layer of the BHJ devices, and its impact on photovoltaic efficiency. Other studies were focused on the vertical phase morphology and its transport process and charge collection in the case of the BHJ is sandwiched between the two electrodes [6]. Indeed, the effect of the interface property on the morphology of the photoactive film has gained immense attention, mainly in the methods on controlling the vertical composition gradient D/A and the alignment of the energy at the BHJ/electrode/substrate interfaces. On the other hand, the use of flexible substrates is limited by the temperature window of annealing. Generally, two synthetic aromatic polyesters, polyethylene terephthalate (PET) and polyethylene naphthalate (PEN)] were previously used for flexible solar cells.[3] In addition, polyimides (PI) were often used as a polymer substrate, which has several advantages such as very high glass transition temperature (about 350^oC) and a competitive permeability compared to other substrates[6, 7]. Unfortunately, PI is not transparent, which is important for solar cells. Sderstrm et. al. [8] have textured the substrate by depositing a back reflector consisting of silver and zinc oxide in order to promote light scattering into the active layer. In addition, Ferekides et. al. [9] have developed flexible foil substrates for CdTe thin film solar cells based on flexible stainless steel (SS) substrate. However, in order to reach high device efficiencies on flexible substrates, further studies on the appropriate processes and materials used in the inverted organic solar cells are needed[9, 10]. Here, we use poly(ethylene-2,6-naphthalate) (PEN) as a substrate which cannot be heated above its glass transition temperature of 125^oC. However, its working temperature spans up to 155^oC[11] and PEN has a very strong resistance to many diluted acids and solvents. On the other hand, permeability and thermal stability (melting temperature of 256^oC) of this aromatic polyester reduce the thermal distortion at the interface and must therefore maintain the integrity of the ZnO (cathode interfacial layer)/ITO(electrode) multilayer and the performance of photovoltaic devices. A detailed study on the impact of the quality of PEN flexible substrate on the morphology of the layers deposited beyond its thermal stability window as well as the interfaces in the layers stack of inverted organic solar cell is necessary.

In this paper we use atom probe tomography (APT), scanning electron microscope (SEM) and microfocus X-rays scattering techniques to analyze the interfaces directly in the OPV device and to obtain a 3D reconstruction of each of the interfaces in a multilayer containing PEN/ITO, ZnO/ITO and P3HT:PCBM/ZnO. In fact, the multilayer PEN-substrate /ITO/ZnO was annealed at a relatively low temperature limited by the polymer thermal stability. Its chemical and thermal stability as well as its crystalline structure was analyzed as a function of annealing temperature (160 and 180^oC). To this end we study and explore the crystalline order in poly(3-hexylthiophene) (P3HT) that has a direct impact on the performance of the OPV device. The performance of the polymer supported solar cells is compared with the one on the rigid substrates (glass) which have been heat treated in the same way. Finally, additional photoluminescence (PL) analysis is used to explore the photophysical properties at the both interfaces (ZnO/P3HT and ZnO/P3HT:PCBM) and the charge transport across active/electron selective layers. This study shows that the thermal activation and expansion through the PEN substrate caused structural and electronic modification of the interfaces in PEN/ITO/ZnO and ZnO/P3HT:PCBM multilayers and therefore the performance of organic photovoltaic devices.

2. EXPERIMENTAL

2.1. Material and device elaboration

The fabrication process of the organic solar cells (OSC) is detailed hereafter. PEN substrates (20 x 20 mm^2, ≤ 15 Ω/sq.) (PECF-IP-Peccel Technologies, Inc.) were first cleaned in an ultrasonic bath with detergent acetone and isopropyl alcohol and deionized water (DI water). UV ozone cleaning was further performed for 30 min. The ZnO target (from Neyco Co.) utilized for sputtering had a 99.999 % purity. ZnO films were deposited on PEN/ITO substrates by RF magnetron sputtering under different deposition conditions such as working pressure, substrate temperature and deposition power[11, 12]. The deposition was carried out in Ar atmosphere at a pressure of 10. 10^{-3} mbar and a constant RF power of 100 W. The substrate temperature was around 40^oC. The ZnO thickness was about 54 nm. After ZnO deposition, one PEN/ITO/ZnO stack (as-prepared sample) was annealed in a quartz tube under a continuous oxygen flow for 1 hour, at different temperatures, between 160 to 180^oC. One as-prepared sample was not annealed and served as a reference. The rest of the stack (P3HT:PCBM/MoO$_x$/Ag) was deposited in identical conditions for all samples. The photoactive layer was deposited on ZnO using spin-coating technique from a **P3HT:PCBM poly(3-hexylthiophene) (P3HT) and [6,6]-phenyl C61 butyric acid methyl ester(PCBM)** solution (1:1 weight ratio in dichlorobenzene) to form a 120 nm-thick layer. The P3HT (98.5% regioregular from Sigma Aldrich GmbH) and the PCBM (PC$_{61}$BM from Nano-C) were used as received without further purification. The PEN/ITO/ZnO/ P3HT:PCBM stacks were then annealed at 140^oC for 15 min under nitrogen atmosphere (in glove box). Finally, MoO$_x$ (99.99 % from Sigma-Aldrich GmbH) and silver (Ag) were deposited sequentially through a shadow mask by thermal evaporation in vacuum at 2. 10^{-6} Torr. The structure of the cells developed in this

study is shown schematically in Fig. 1. The thickness of MoO_x and Ag are found to be around 5 and 120 nm, respectively. Device active area was about 9 mm^2. For comparison the OSC devices were also prepared using rigid substrate and following the same procedure, based ITO-coated glass substrates from Przisions Glass & Optik GmbH, Germany (CEC20S, $\leq$ 20 Ω /sq., 20 x 20 mm^2).

2.2. Device characterization

X-ray diffraction (XRD) was performed using a Rigaku SmartLab diffractometer (200 mA, 45 kV) equipped with a Ge (220)x2 monochromator and using $CuK\alpha 1$ incident radiation (λ= 0.154056 nm). Symmetric ω - 2θ scans were done on the OSC devices

Synchrotron-based micro-focus X-ray diffraction (SR-μXRD) measurements were carried out at the ID13 beamline of the ESRF. The monochromatic X-ray beam with the wavelength of 1.0Å was focused down to 1 μm along both axes using crossed Fresnel optics. The X-ray patterns were recorded with a FreLon fast CCD camera with a pixel size of 50 μm. The norm of the scattering vector $\mathbf{s}$ ($|\mathbf{s}|$=2$\sin\theta/\lambda$) was calibrated using the diffraction peaks of corundum. The regions of interest on the sample were selected with an on-axis optical microscope operated in reflection mode. More technical details concerning applications of micro-focus X-ray scattering to studies of the semicrystalline polymer structure has been done by Ivanov et al.[13] The free-standing OSC devices mounted on a glass capillary were scanned with the help of an x-y gantry in transmission geometry (Fig. S1 in Supplementary material) in order to analyze the micro-structure of each individual layer in the stack as a function of thickness. The diffraction patterns were collected using a step of 2 μm. The data reduction and analysis including background correction, visualization and radial as well as azimuthal integration of the 2D diffractograms were performed using home-built routines designed in Igor Pro software (Wavemetrics Ltd.).

Atom probe tomography (APT). APT specimens (sharp tips) were prepared by lift-out method and standard milling [14] using a dual beam ZEISS Nvision 40. In order to reduce Ga implantation and avoid damages in the region of interest, the multilayered P3HT:PCBM/ZnO/ITO/PEN stack was capped with about 800 nm of Pt and a final polishing was performed at low acceleration voltage (2 kV). The tips were analyzed by laser-assisted wide-angle tomographic atom probe (LAWATAP) from CAMECA at 80 K in an ultrahigh vacuum chamber at a pressure of 10^{-10}) mbar. Specimens were then field evaporated using 350 fs laser pulses (wavelength: λ= 342 nm)

Current density-voltage (J-V) characteristics of the OSCs were measured with a HP Agilent source measurement unit, under darkness and light exposure. For the latter, a solar simulator under AM 1.5 G conditions (Oriel Xenon 150 W) was used. The light intensity was calibrated with a standard silicon solar cell using a light intensity of 100 $mW.cm^{-2}$). The device performances were measured under nitrogen atmosphere.

Differential scanning calorimetry (DSC). The measurements were performed using a Q1000 DSC from TA Instruments (New Castle, DE) with a heating rate of $5^oC.min^{-1}$. Empty aluminium pans were used for the sample and reference. Initially, the calorimeter baseline was determined using a sapphire standard sample. The temperature of the calorimeter was calibrated from the observed melting points of ultra-pure materials as stearic acid, indium and tin.

Photoluminescence (PL) analysis. PL experiments presented herein were conducted at room temperature using a 532 nm laser (10 mW) modulated at a frequency of 15 kHz as excitation source. The sample luminescence was collected by an optical fiber and analyzed by a CCD camera.

3. RESULTS AND DISCUSSIONS

3.1. Morphological and micro-structure of the PEN/ITO, ZnO/ITO and ZnO/P3HT:PCBM interfaces

In inverted organic solar cells, the interfacial contact between the substrate and the electrode (ITO) and that of the cathode buffer layer (ZnO) plays important role in the electron transport. In this part, we focus on the interface morphology of PEN/ITO and ITO/ZnO. Under thermal annealing, PEN substrate affects the arrangement of ITO deposited above, and consequently on ZnO particles beside ITO by the diffusion effect as well as the interface of P3HT:PCBM/ZnO, that can result in the hole blocking and affect the device performance. Furthermore, it is essential to study the disposition of the ZnO/ITO interface and adjacent PCBM:P3HT mixture layer directly in the cell. For this purpose a micro-sample with multiple layers (a part with P3HT:PCBM, ZnO and ITO layers) taken from the as-prepared cell were prepared by FIB/SEM for atom probe tomography, in order to have a three-dimensional reconstruction of ZnO/ITO and P3HT:PCBM/ZnO multilayer. Fig. 2a displays the tip shape specimen prepared from the studied heterostructure by focused ion beam milling. The 3D reconstruction of the analyzed volume is shown in Fig. 2b. The spatial distribution of single and molecular ions species are clearly observable. Position of the light elements (H and C atoms) presented mainly in the organic layer of P3HT:PCBM cannot be determined accurately. Nevertheless, a dominant monoatomic ion of the atomic carbon (C+, C2+)[15] characteristic of the mixture of P3HT/PCBM, have been detected (Fig. S2 in Supplementary material). However, a moderate atomic mass ions are completely absent from the mass spectrum. Indeed, evaporation of large molecular ions can be problematic for 3D reconstructions of the vertical composition gradient PCBM aggregates and P3HT crystallite. From the phase separation in the P3HT:PCBM layer near ZnO, as information about the structure and orientation of the
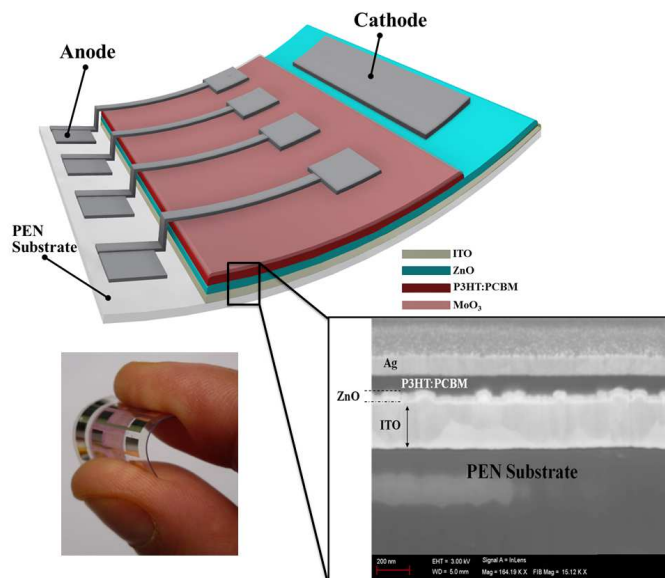
Figure 1: Schematic illustration of inverted organic solar cell (OSC) with cross-section scanning electron microscope (SEM) image for non-annealed stack (PEN/ITO/ZnO/P3HT:PCBM/MoO_x/Ag)
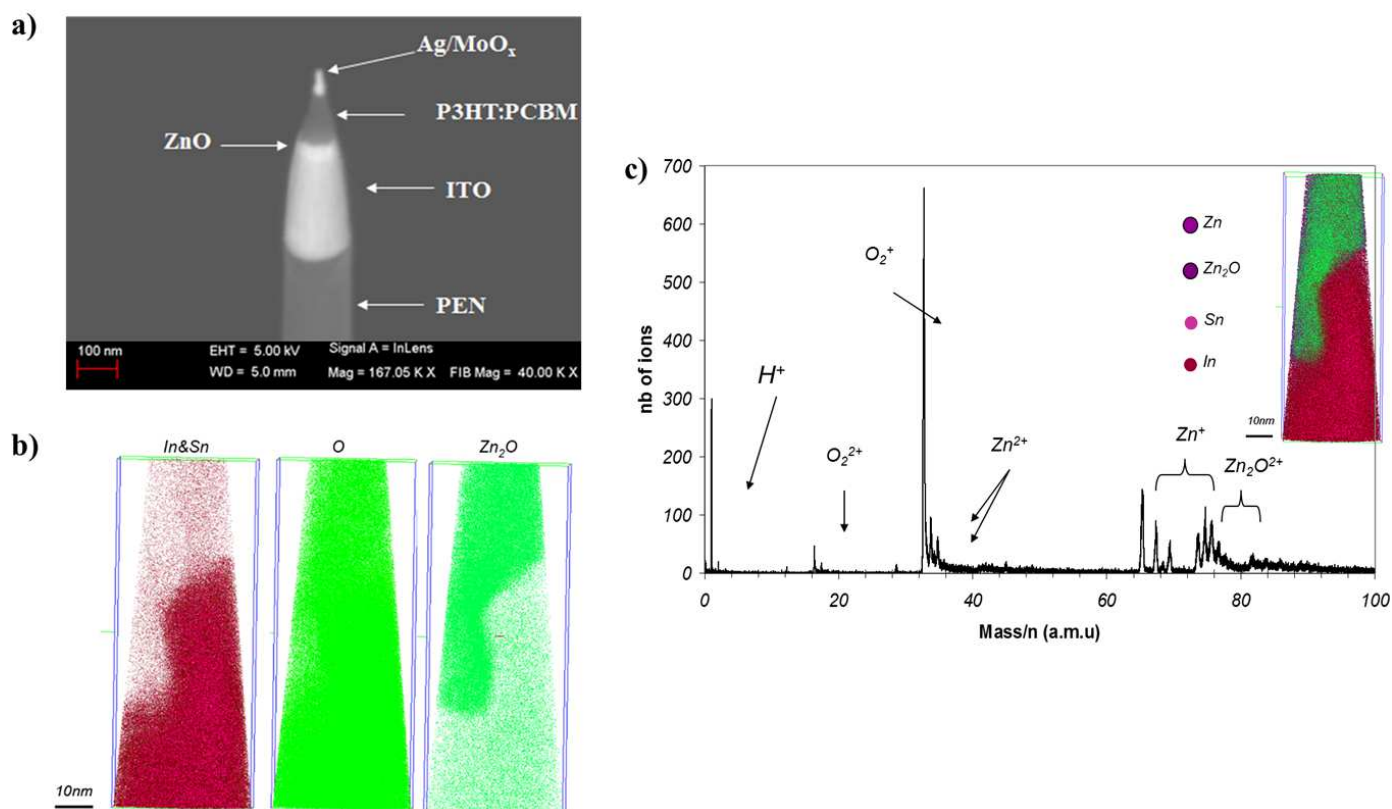

Figure 2: Atom probe tomography imaging of as-grown ZnO/ITO multilayer beside P3HT:PCBM layer. a) SEM micro-sample specimens of each layer in OSC structure. b) ZnO and ITO layers cartography. C) Mass spectrum micro-sample specimens focuses on ZnO and ITO films.

molecular ion is lost, effectively reducing the spatial resolution and thus not allow us to conclude about the chemistry spatial distribution near this interface. However, the spatial distribution of the other elements: In, Sn, Zn and O can be measured and studied (Fig. 2b and c). Our data indicate that inside layers the distribution of all these species is homogeneous. One can observe in Fig. 1 and Fig. 2b that the interface between ITO and ZnO layers is not sharp. In fact, a modulation of the chemical composition at the ITO/ZnO interface is observed due to a significant
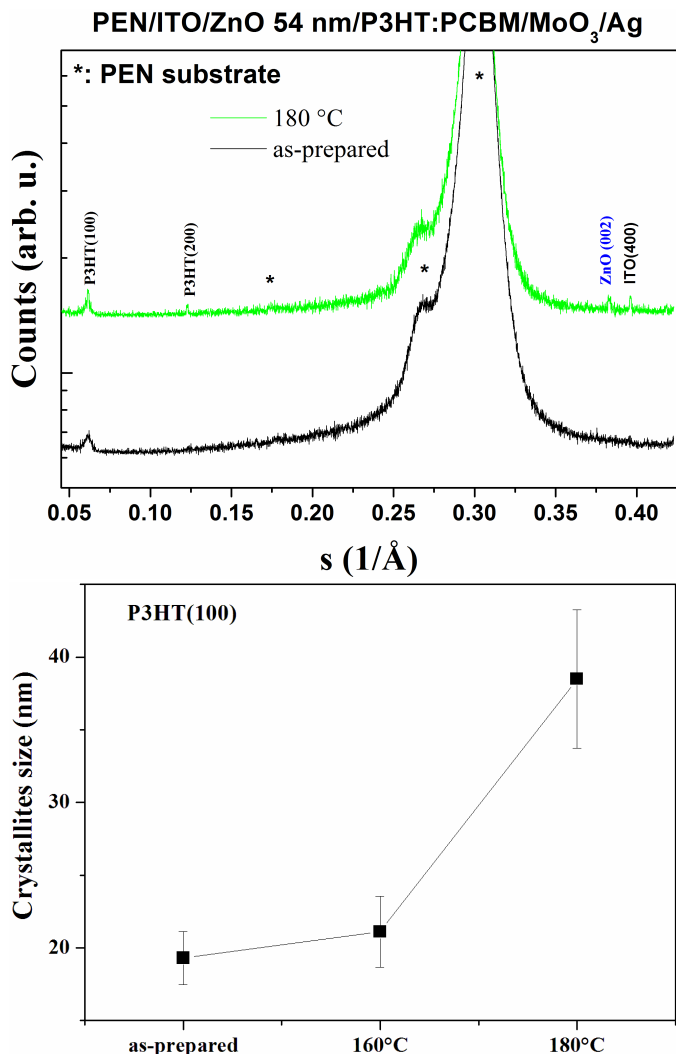
4

PEN/ITO/ZnO 54 nm/P3HT:PCBM/MoO$_3$/Ag

Figure 3: Effect of annealing on the OSC device studied by XRD a) XRD patterns of PEN/ITO/ZnO/P3HT:PCBM/ MoO$_x$/Ag heterostructure for the as-grown and annealed at 180°C ZnO layer. b) Change of the P3HT crystallites size as a function of ZnO annealing temperature for cells prepared on PEN substrate

rough interface which should strongly affect the interfacial roughness of the P3HT:PCBM organic layer, which is in agreement with the SEM observations in Fig. 1. These structural defects should mainly influence the interfacial molecular order of P3HT near ZnO layer and as a result the loss of electrons caused by charge recombination at defect sites[16]. Such ordered profile promotes the vertical phase segregation and enhances the carrier mobility which should influence the charge transport and series resistance of photovoltaic cells and its performances [5, 16].

3.2. Structural characteristics of PEN substrate, ZnO and P3HT

X-ray diffraction patterns recorded on PEN/ITO/ZnO/P3HT:PCBM/MoO$_x$ heterostructure for the as-grown and annealed at 180°C interfacial ZnO layer are displayed in Fig. 3a. The sample with ZnO annealed at 180°C ex-

hibits different diffraction peaks which can be assigned to ITO, ZnO, and P3HT evidencing the well-defined crystalline structure of these layers. For the non-annealed samples, theses peaks are hardly visible showing that annealing improves the crystallinity of the main layers. The peak around the **s** of 0.38$\mathring{A}$ $^{-1}$ in Fig. 3a was identified as 002 reflection of the hexagonal wurzite form of ZnO. For the as-prepared ZnO, the 002 is very weak, which is indicative of a largely amorphous character of the non-annealed ZnO layer. Upon annealing at 180°C, the 002 peak intensity significantly increases, and shows a preferred orientation of ZnO layer with the c-axis perpendicular to the PEN substrate. Contrary to other layers, the crystallinity of ZnO is greatly affected by annealing. The grain orientation in the c-axis direction is related to minimization of the free surface energy density of the film and its interface with the PEN/ITO substrate. The grain orientation in the c-axis direction is related to minimization of the free surface energy density of the film and its interface with the PEN/ITO substrate. Thus evolution of ZnO crystalline peaks will accompany that of ITO showing that the two phenomena of crystal growth are linked and continues.[17] Fig. 3b displays the change of P3HT crystallites size in the P3HT:PCBM layer calculated using Debye-Scherrer formula from the 100 peak of P3HT observed at **s** of 0.062$\mathring{A}$ $^{-1}$ (Fig. 3a). As can be observed, the crystallite size increases slowly with increasing annealing temperature at a first stage from as-grown to 160°C, while the crystallite size increases more rapidly at higher annealing temperature (180°C). The increase in annealing temperature of ZnO/ITO/PEN multilayer leads to an increase in motion of polymer molecules and chain mobility, which grown above.[18] Therefore, the P3HT forms larger crystals when deposited on highly crystalline ZnO. The second diffraction peak of P3HT crystals observed at 0.124$\mathring{A}$ $^{-1}$ and indexed as 200 appears after annealing at 180°C, in addition to the (100) peak. These 00l peaks reveal straightened lamellar stacking with a slightly larger lattice spacing of 16.4 $\mathring{A}$, which can be associated with the interdigitated alkyl chains[19, 20]. The transformation and expansion of the PEN substrate (Tg approaching 125°C for PEN substrate as shown in Fig. S3 in Supplementary material) facilitates the ZnO crystal growth and consequently, the enhanced orientation of P3HT lamellae along the edge-on of the surface normal direction. Note that the anisotropic texture and good P3HT and ZnO crystals orientation lead to a significant change in the characteristics of the photovoltaic devices. The most intense peaks around 0.25-0.35$\mathring{A}$ $^{-1}$ in Fig. 3a were indexed as 100 and 110 peaks of the α-crystal modification of PEN (i.e. the material of the substrate) [21]. This peak is almost not influenced by annealing that indicates the structural stability of the flexible substrate used in this study. The 1D XRD analysis does not allow probing the possible anisotropy of the OPV device layers. Therefore 2D SR-μXRD scans of the OPV cross sections were carried out (cf. Fig. S1 in Supplementary material) for two samples: PEN/ITO substrate
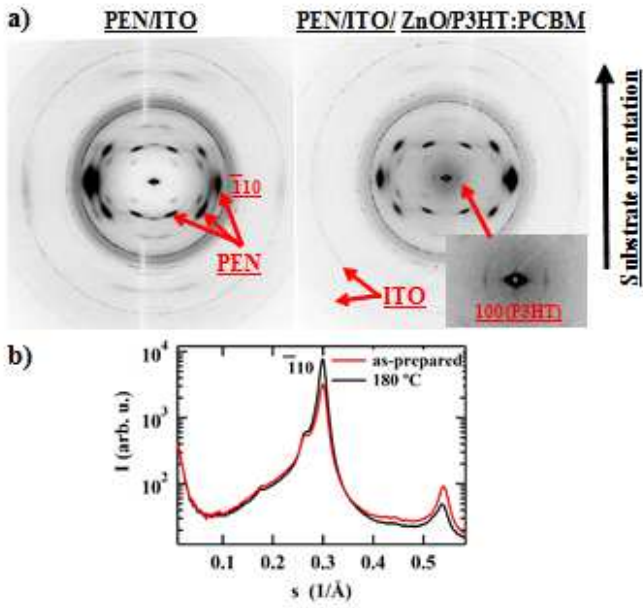
Figure 4: 2D μXRD images of P3HT/ZnO/ITO/PEN and PEN/ITO samples. The substrate orientation is vertical. b) Comparison of the 1D μXRD equatorial profiles of PEN substrate corresponding to the same thickness (60μm from the surface) for the as-prepared and annealed at 180°C ZnO layer

and P3HT:PCBM/ZnO/ITO/PEN structure annealed at 180°C. Fig. 4a compares the 2D μXRD patterns taken at the surface of as-prepared ITO/PEN sample and the surface after P3HT deposition on ZnO/ITO/PEN multilayer stack that was annealed at 180°C. One can see the typical fiber-like pattern[22, 23] indicating that the as-received flexible PEN substrate is highly oriented with its polymer backbone directed along the substrate surface and the normal to the substrate being along the 1-10 reciprocal-space vector of the PEN unit cell. The 1D XRD and 2D SR-μXRD are in good agreement. The well-oriented 100 peak of P3HT with d $\approx$ 16.4 Å has equatorial orientation, which means that the P3HT chains are parallel to the PEN substrate and arranged with the molecular planes perpendicularly to the substrate. Fig. 4b compares the equatorial SR-μXRD profiles corresponding to the same thickness (i.e. at ca. 60μm distance from the surface) for PEN substrate as prepared and annealed at 180°C. Note that the crystalline structure and degree of orientation of the PEN substrate is unchanged after annealing at 180°C, a temperature above its Tg. Therefore, one can conclude that the crystalline structure and texture of the poly(ethylene-2,6-naphthalate) substrate is not affected by the annealing at 180°C.

3.3. Electrical and Photophysical characterization of PEN and ZnO/P3HT:PCBM interface

The performance of our photovoltaic devices, J-V curves under illumination conditions were carried out (Fig. 5). The corresponding photovoltaic performances are summarized in Table 1. Fig. 5 shows the results obtained for

flexible device (PEN substrate) and rigid device (glass substrate). In case of non-annealed substrate of PEN/ITO/ZnO multilayer, we obtained S-shape in J-V curve for both substrates. Annealing PEN/ITO/ZnO multilayer at 180°C reduces the S-shape in J-V characteristics for flexible substrate, reaching an open circuit voltage Voc around 0.59V for both substrates. **The S-shaped characteristics observed for as-prepared samples can be explained by the poor conductivity of ZnO as-prepared compared to annealed samples and also by the defect interface P3HT/ZnO, which can promote poor charge transport and high value of the series resistance (Rs) until 83 Ω.cm^2 for as-prepared sample (see Table 1 and Table 2). Moreover, the phenomenon of "counter-diode" could be induced by the phase separation effects of P3HT and PCBM beside ZnO. By annealing ZnO, these effects can induce more appropriate phase separation between P3HT and PCBM, which facilitates exciton dissociation and charge transport to the cathode. The latter can explain the decrease of Rs for the annealed sample at 180 ^{o}C which has almost reached its soil value (15 Ω.cm^2) and its higher fill factor (FF) about 48%, compared to the as- Prepared.** On the other hand, for both flexible and rigid substrate the efficiency values are higher for annealing at 180°C and almost similar (1.5%) with open circuit voltage value of 0.54V, for device with as-prepared PEN/ITO/ZnO multilayer substrate. More interestingly, in case of flexible substrate, annealing at 180°C contributes mostly to improve the performance, therefore a perfect diode characteristic in its J-V curve. This is accompanied by a sharp increase in fill factor (FF) up to 49% compared to the value of 33% obtained for as prepared PEN/ITO/ZnO multilayer substrate. The short-circuit current density (Jsc) is higher for PEN/ITO/ZnO multilayer annealed at 180°C (7.67 mA/cm) and its efficiency attain up to 2.18 %. Indeed, the J-V characteristic for the device made on PEN substrate with PEN/ITO/ZnO multilayer annealed at 180°C is not perfect with a ligther S-shaped behavior located towards the x-axis (Voltage) compared to that on rigid substrate. To clarify this point, we have measured the conductivity of the ITO layer on PEN substrate before and after annealing (160 and 180°C) as shown in Table 2. It is found that the conductivity decreases for the PEN/ITO substrate annealed at 180°C. This decrease can partly explain the decrease in photovoltaic performance for device compared to that at 160 ^{o}C, knowing that the series resistance remained the same about 15 Ω.cm^2.

In fact, according to Atom probe tomography in section A, thermal energy produced by annealing treatment was transferred to ZnO layer which favor reorganization of surface to find the most stable state and a more homogeneous structure, which contributes to the spread of the particles of ITO and ZnO giving rise to an increase of crystallites size (20 nm) as calculated from XRD data. In order to go further to explain this mechanism, the mea-

Table 1: SUMMARY OF THE PHOTOVOLTAIC PARAMETERS OF INVERTED OPVS INTEGRATING ZnO CATHODE WITH NO ANNEALING AND ANNEALING AT DIFFERENT TEMPERATURES

Substrate	Sample	Voc (V)	Jsc (mA/cm^2)	FF(%)	η(%)	$R_s(\Omega.cm^2)$	$R_{sh}(\Omega.cm^2)$
glass	As-prepared	0.59	7.36	31.38	1.29	30	111
	180°C	0.59	9.067	47.25	2.54	15	324
PEN	As-prepared	0.54	5.53	32.85	1.5	83	328
	160°C	0.57	9.17	49.18	2.58	15	449
	180°C	0.58	7.67	48.75	2.18	15	512

Table 2: SUMMARY OF THE HALL EFFECT MEASURMENTS OF PEN/ITO, NO ANNEALED AND ANNEALED AT DIFFERENT TEMPERATURES (160 AND 180°C)

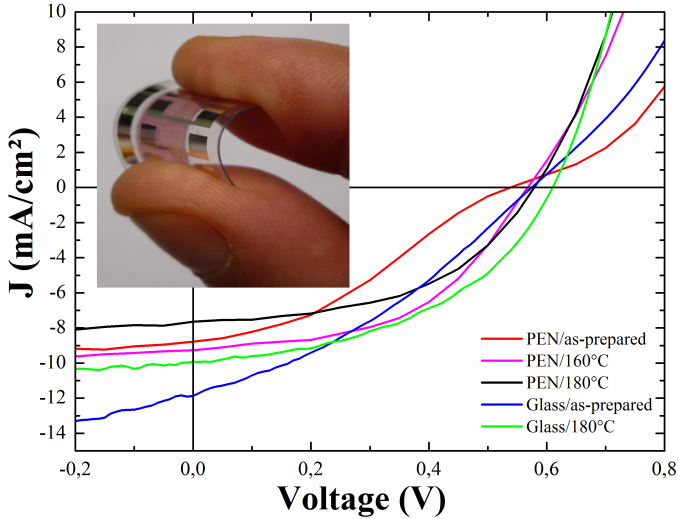| Sample	Bulk concentration (cm^{-3})	Resistivity (Ω.cm)	Mobility (cm^2/V.s)	Roughness (rms)
PEN/ITO As-prepared	1.39 x 10^{21}	1.27 x 10^{-4}	35.3	-
PEN/ ITO 160°C	1.36 x 10^{21}	1.26 x 10^{-4}	35.4	3.8 nm
PEN/ ITO 180°C	1.28 x 10^{21}	1.56 x 10^{-4}	31.2	4 nm

Figure 5: J-V characteristics of the both substrate (PEN/glass)/ITO/ZnO/P3HT:PCBM/MoO$_x$/Ag structure without and with annealing ZnO at 160 and 180°C, under illumination

surements of differential scanning calorimetry (DSC) were carried out and allowed us to visualize the exothermic peak corresponding to the crosslink of PEN and also selecting the working temperature range of our substrate. We find that the glass transition temperature (Tg) was clearly detectable at about 130°C as shown in Fig. S3 in Supplementary material. Thus, the temperature above 130°C will change the crystalline state of PEN substrate as evidenced by Hardy et al. [24] who investigated mechanical relaxation behavior of dynamic for semi-crystalline oriented PEN films and observed an increase in the degree of crystallinity due to an increase in grain size. Indeed, once P3HT grows on ZnO layer, its growth is on large ZnO grains, which induces an increase in grain size

of P3HT as shown previously in Fig. 3b. In addition, P3HT crystallite size increases sharply during annealing at 180°C, since a value of 40 nm is obtained. Jouane et al.[19] have shown that this sharp increase will induce a significant decrease in the density at the interfaces of the active layer shown by the heterojunction donor/accepter based on P3HT: PCBM (that means the surface area to volume ratio), which will result in a reduction of the photocurrent generated by the device at 180°C. Such a process could therefore explain the drop in short-circuit current density (Jsc) observed on flexible substrate annealed at 180 ^{o}C compared to that at 160 ^{o}C. This should limit PCBM diffusion within ZnO layer, which can explained the decline in photovoltaic performance to 180°C. Finally, we conclude that the thermal stability of PEN substrate can also contribute to change the surface quality which can affect the growth of upper layers (ITO and ZnO) and thus the photoactive polymer. However, this stability naturally beneficial to the crystallization of ZnO and ITO (Fig. 3), and thus to the interfacial stability, ITO conductivity and ZnO surface roughness (Fig. 2). This latter can have an adverse consequence on contact beside active layer P3HT:PCBM/ZnO. In order, to clarify this point, the PL spectra of P3HT, P3HT/ZnO, P3HT:PCBM/ZnO (20, 54 and 100 nm) and P3HT:PCBM were measured to assess the state of interactions between the different layers in the device at the excited state which can provide evidence of the exciton recombination within different interfaces. Note that the PL experiments were repeated and normalized with respect to the optical density. Fig. 6 displays the PL spectra for each case previously mentioned. The laser excitation is close to the maximum absorption peak of P3HT (550 nm), and far to the absorption peak of ZnO. As can be observed, three emission peaks of P3HT centered at 648 nm 710 and 780 nm, which correspond to

the vibronic structures of P3HT. The PL emission peak at about 648 nm (1.91 eV) is associated with pure electronic transition of P3HT and the peaks at 710 nm (1.74 eV) to the first vibronic band[25–27]. However, the PL emission at 780 nm (1.5 eV) shows an order in the lamellar structure of P3HT, which could promote vertical segregation of P3HT and PCBM molecules and as a consequence the electronic communication between the donor and acceptor layers. Therefore, the charge transfer and transport until ZnO cathode interfacial layer will be facilitated. In addition, the PL intensity for ZnO/P3HT:PCBM continuously increases with increasing ZnO thickness (20, 54 and 100 nm). The exact mechanism of this behavior in exciton dissociation rate is uncertain and could be linked to defects induced by ZnO thickness increase. Note that the PL intensity was totally quenched in P3HT:PCBM thin films indicating a very effective charge transfer between P3HT and PCBM. Moreover, the PL intensity was not fully quenched in ZnO/P3HT double layers, but a slight decrease in luminescence compared to that observed for pure P3HT, which indicates a negligible charge transfer from P3HT to ZnO. Indeed, the difference in dissociation efficiency of excitons in the various interfaces can also be explained by the difference in lifetime of excitons obtained by PL lifetime, as was reported by Lin, et al.[28] who showed that τ_{P3HT} as larger than $\tau_{ZnO/P3HT}$. This can be understood by a fast non-radiative process of photogenerated excitons at the ZnO/P3HT interface. Most of photogenerated excitons carriers will be separated at the P3HT and PCBM interface and only a tiny fraction of excitons will be separated at the P3HT/ ZnO interface for this reasons we have a lower PL intensity observed in ZnO/P3HT. Furthermore, the PL intensity quenching observed in the (ZnO/P3HT:PCBM) for 20-nm-thick ZnO is a bit stronger than that observed for 54 and 100 nm, which is a signature of a better efficiency of transfer of charge at the interface P3HT:PCBM/ZnO (20nm). In order to investigate the electronic structure at the ZnO/P3HT:PCBM interface and the influence of ZnO annealing on its work function we consider that the HOMO and LUMO levels of P3HT and PCBM will not be influenced by ZnO annealing, but instead by the exchange at the P3HT:PCBM/ZnO interface. The change in optical gap (Eg) of ZnO by annealing can influence the charge transport at the interface P3HT:PCBM/ZnO, and as a result can disrupt the interfacial molecular order of P3HT at the interface with ZnO. Indeed, we carried out optical transmission measurements to extract Eg of ZnO in a glass/ITO/ZnO stack. We found a small variation in Eg (around 3.25 eV) for samples: without and with annealing at 180^oC. These results show that the influence of ZnO Eg is not significant and that thermal annealing of PEN substrate affect the morphology and the surface roughness of ZnO layer.
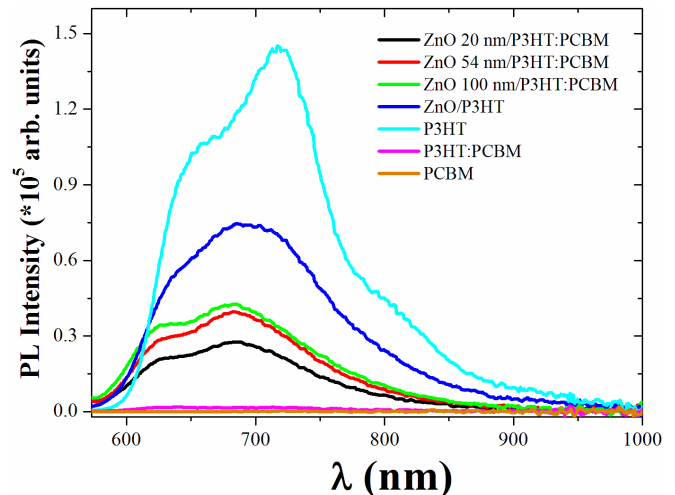

Figure 6: PL spectra of P3HT, P3HT:PCBM, P3HT/ZnO, P3HT:PCBM/ZnO and PCBM films. b) Gaussian band fits of P3HT/ZnO by using an excitation wavelength of 532 nm in the range from 500 to 900 nm

4. CONCLUSION

In summary, we have studied the interface morphology and the micro-structural modification of each layer of the BHJ devices, and their impact on photovoltaic efficiency. The growth of ZnO films on flexible substrates and application of thermal annealing at 140-180^oC for flexible substrates (PEN/ITO) induce a change in the vertical composition gradient of the PCBM aggregates and P3HT crystallites in P3HT:PCBM film in the proximity of ZnO. This change takes into account the thermal expansion of the flexible substrates and the induced energy, which contributes to the diffusion of the ITO and ZnO particles increasing the size of these crystallites. Indeed, this expansion is combined with a better organization of P3HT polymer chains which would favor the diffusion of PCBM at the interface with ZnO. Consequently, the thermal activation of the charges up to 160 ^oC at the ZnO/P3HT:PCBM interface led to a strong recovery of the performance of the cells, reaching values quite comparable to those obtained with rigid substrates. We finally succeeded to directly correlate the morphology of the interfaces with the micro-structural and electronic modification of the interfaces of PEN/ITO/ZnO and ZnO/P3HT:PCBM multilayer and therefore with the performance of the flexible organic photovoltaic devices.

ACKNOWLEDGMENTS

References

[1] P. Lper, B. Niesen, S. J. Moon, S. M. de Nicolas, J. Holovsky, Z. Remes, M. Ledinsky, F. J. Haug, J. H. Yum, S. D. Wolf, C. Ballif, Organicinorganic halide perovskites: Perspectives for silicon-based tandem solar cells, IEEE Journal of Photovoltaics 4 (6) (2014) 1545–1551. `doi:10.1109/JPHOTOV.2014.2355421`.

[2] Y. Liu, N. Qi, T. Song, M. Jia, Z. Xia, Z. Yuan, W. Yuan, K.-Q. Zhang, B. Sun, Highly flexible and lightweight organic solar cells on biocompatible silk fibroin, ACS Applied Materials & Interfaces 6 (23) (2014) 20670–20675. `doi:10.1021/am504163r`.

[3] K. Vandewal, K. Tvingstedt, A. Gadisa, O. Inganäs, J. V. Manca, Relating the open-circuit voltage to interface molecular properties of donor:acceptor bulk heterojunction solar cells, Phys. Rev. B 81 (2010) 125204. `doi:10.1103/PhysRevB.81.125204`.

[4] H. W. Ro, B. Akgun, B. T. O'Connor, M. Hammond, R. J. Kline, C. R. Snyder, S. K. Satija, A. L. Ayzner, M. F. Toney, C. L. Soles, D. M. DeLongchamp, Poly(3-hexylthiophene) and [6,6]-phenyl-c61-butyric acid methyl ester mixing in organic solar cells, Macromolecules 45 (2014) 6587–6599. `doi:10.1021/ma3008527`.

[5] R. C. Masters, A. J. Pearson, T. S. Glen, F.-C. Sasam, L. Li, M. Dapor, A. M. Donald, D. G. Lidzey, C. Rodenburg, Subnanometre resolution imaging of polymerfullerene photovoltaic blends using energy-filtered scanning electron microscopy, Nature Communication 6 (2015) 6928. `doi:10.1038/ncomms7928`.

[6] R. Noriega, J. Rivnay, K. Vandewal, F. P. V. Koch, N. Stingelin, P. Smith, M. F. Toney, A. Salleo, A general relationship between disorder, aggregation and charge transport in conjugated polymers, Nature Materials 12 (2013) 1038–1044. `doi:doi:10.1038/nmat3722`.

[7] C.-S. Ha, A. S. Mathews, Polyimides and High Performance Organic Polymers, Springer Berlin Heidelberg, Berlin, Heidelberg, 2011, pp. 1–36. `doi:10.1007/978-3-642-19077-3_1`.

[8] K. Sderstrm, J. Escarr, O. Cubero, F.-J. Haug, S. Perregaux, C. Ballif, Uv-nano-imprint lithography technique for the replication of back reflectors for n-i-p thin film silicon solar cells, Progress in Photovoltaics: Research and Applications 19 (2) (2011) 202–210. `doi:10.1002/pip.1003`.
URL `http://dx.doi.org/10.1002/pip.1003`

[9] V. Palekis, V. Guntur, D. Hodges, D. Morel, E. Stefanakos, C. Ferekides, Substrate based cdte solar cells fabricated on metallic foils: Device, material, and processing issues, in: Photovoltaic Specialists Conference (PVSC), 2011 37th IEEE, 2011, pp. 002779–002783. `doi:10.1109/PVSC.2011.6186523`.

[10] W. A. MacDonald, J. M. Mace, Flexible Substrate Requirements for Organic Photovoltaics, Wiley-VCH Verlag GmbH & Co. KGaA, 2014, pp. 513–538. `doi:10.1002/9783527656912.ch17`.
URL `http://dx.doi.org/10.1002/9783527656912.ch17`

[11] T. Higashioji, T. Tsunekawa, B. Bhushan, Mechanical property and dimensional stability of substrates for magnetic tapes, Tribology International 36 (46) (2003) 437 – 445, tribology of Information Storage Devices 2001. `doi:http://dx.doi.org/10.1016/S0301-679X(02)00232-3`.

[12] Y. Jouane, S. Colis, G. Schmerber, P. Kern, A. Dinia, T. Heiser, Y.-A. Chapuis, Room temperature zno growth by rf magnetron sputtering on top of photoactive p3ht:pcbm for organic solar cells, J. Mater. Chem. 21 (2011) 1953–1958. `doi:10.1039/C0JM02354J`.

[13] M. Rosenthal, M. Burghammer, G. Bar, E. T. Samulski, D. A. Ivanov, Switching chirality of hybrid left right crystalline helicoids built of achiral polymer chains when right to left be-

[14] K. Thompson, D. Lawrence, D. Larson, J. Olson, T. Kelly, B. Gorman, In situ site-specific specimen preparation for atom probe tomography, Ultramicroscopy 107 (23) (2007) 131 – 139. `doi:http://dx.doi.org/10.1016/j.ultramic.2006.06.008`.

[15] T. PROSA, S. K. KEENEY, T. KELLY, Atom probe tomography analysis of poly(3-alkylthiophene)s, Journal of Microscopy 237 (2) (2010) 155–167. `doi:10.1111/j.1365-2818.2009.03320.x`.
URL `http://dx.doi.org/10.1111/j.1365-2818.2009.03320.x`

[16] Y. Jouane, S. Colis, G. Schmerber, C. Leuvrey, A. Dinia, P. Leveque, T. Heiser, Y.-A. Chapuis, Annealing treatment for restoring and controlling the interface morphology of organic photovoltaic cells with interfacial sputtered zno films on p3ht:pcbm active layers, J. Mater. Chem. 22 (2012) 1606–1612. `doi:10.1039/C1JM13569D`.
URL `http://dx.doi.org/10.1039/C1JM13569D`

[17] H.-C. Lee, O. O. Park, The evolution of the structural, electrical and optical properties in indium-tin-oxide thin film on glass substrate by {DC} reactive magnetron sputtering, Vacuum 80 (8) (2006) 880 – 887. `doi:http://dx.doi.org/10.1016/j.vacuum.2005.11.069`.

[18] C. B. Roth, J. R. Dutcher, Glass transition and chain mobility in thin polymer films, Journal of Electroanalytical Chemistry 584 (1) (2005) 13 – 22. `doi:http://dx.doi.org/10.1016/j.jelechem.2004.03.003`.

[19] Y. Jouane, S. Colis, G. Schmerber, A. Dinia, P. Lvque, T. Heiser, Y.-A. Chapuis, Influence of flexible substrates on inverted organic solar cells using sputtered zno as cathode interfacial layer, Organic Electronics 14 (2013) 1861 – 1868. `doi:http://dx.doi.org/10.1016/j.orgel.2013.04.024`.
URL `http://www.sciencedirect.com/science/article/pii/S1566119913001833`

[20] G. Li, V. Shrotriya, J. Huang, Y. Yao, T. Moriarty, K. Emery, Y. Yang, High-efficiency solution processable polymer photovoltaic cells by self-organization of polymer blends, Nature Materials 4 (2005) 864–868. `doi:doi:10.1038/nmat1500`.

[21] C. van den Heuvel, E. Klop, Relations between spinning, molecular structure and end-use properties of polyethylene naphthalate tyre yarns, Polymer 41 (11) (2000) 4249 – 4266. `doi:http://dx.doi.org/10.1016/S0032-3861(99)00554-6`.

[22] J. R. May, C. Gentilini, D. E. Clarke, Y. I. Odarchenko, D. V. Anokhin, D. A. Ivanov, K. Feldman, P. Smith, M. M. Stevens, Tailoring of mechanical properties of derivatized natural polyamino acids through esterification and tensile deformation, RSC Adv. 4 (2014) 2096–2102. `doi:10.1039/C3RA44865G`.

[23] Y. I. Odarchenko, D. V. Anokhin, D. Doblas, M. Rosenthal, J. J. Hernandez, L. Vidal, N. J. Sijbrandi, A. J. Kimenai, E. P. C. Mes, R. Broos, G. Bar, P. J. Dijkstra, J. Feijen, M. Soloviev, D. A. Ivanov, Primary chemical sequence ultimately determines crystal thickness in segmented all aliphatic copolymers, Macromolecules 47 (22) (2014) 7890–7899. `doi:10.1021/ma501545b`.

[24] L. Hardy, I. Stevenson, A. Fritz, G. Boiteux, G. Seytre, A. Schnhals, Dielectric and dynamic mechanical relaxation behaviour of poly(ethylene 2,6-naphthalene dicarboxylate). ii. semicrystalline oriented films, Polymer 44 (15) (2003) 4311 – 4323. `doi:http://dx.doi.org/10.1016/S0032-3861(03)00332-X`.

[25] Y. Song, C. Hellmann, N. Stingelin, G. D. Scholes, The separation of vibrational coherence from ground- and excited-electronic states in p3ht film, The Journal of Chemical Physics 142 (21). `doi:http://dx.doi.org/10.1063/1.4916325`.

[26] S. Cook, A. Furube, R. Katoh, Analysis of the excited states of regioregular polythiophene p3ht, Energy Environ. Sci. 1 (2008) 294–299. `doi:10.1039/B805643A`.

[27] J. A. McLeod, A. L. Pitman, E. Z. Kurmaev, L. D. Finkelstein, I. S. Zhidkov, A. Savva, A. Moewes, Linking the homo-lumo gap to torsional disorder in p3ht/pcbm blends, The Journal of Chemical Physics 143 (22). `doi:http://dx.doi.org/10.1063/1.4936898`.

[28] Y.-Y. Lin, C.-W. Chen, T.-H. Chu, W.-F. Su, C.-C. Lin,

C.-H. Ku, J.-J. Wu, C.-H. Chen, Nanostructured metal oxide/conjugated polymer hybrid solar cells by low temperature solution processes, J. Mater. Chem. 17 (2007) 4571–4576. doi:10.1039/B710400F.